crystals

MDPI

Article

Elastodynamics Field of Non-Uniformly Moving Dislocation: From 3D to 2D

Shichao Luo and Yinan Cui *

Applied Mechanics Laboratory, School of Aerospace Engineering, Tsinghua University, Beijing 100084 China; luosc20@mails.tsinghua.edu.cn

* Correspondence: cyn@mail.tsinghua.edu.cn

Abstract: Molecular dynamics (MD) and experiments indicate that the high-speed dislocations dominate the plasticity properties of crystal materials under high strain rate. New physical features arise accompanied with the increase in dislocation speed, such as the "Lorentz contraction" effect of moving screw dislocation, anomalous nucleation, and annihilation in dislocation interaction. The static description of the dislocation is no longer applicable. The elastodynamics fields of non-uniformly moving dislocation are significantly temporal and spatially coupled. The corresponding mathematical formulas of the stress fields of three-dimensional (3D) and two-dimensional (2D) dislocations look quite different. To clarify these differences, we disclose the physical origin of their connections, which is inherently associated with different temporal and spatial decoupling strategies through the 2D and 3D elastodynamics Green tensor. In this work, the fundamental relationship between 2D and 3D dislocation elastodynamics is established, which has enlightening significance for establishing general high-speed dislocation theory, developing a numerical calculation method based on dislocation elastodynamics, and revealing more influences of dislocation on the macroscopic properties of materials.

Keywords: dislocation dynamics; elastodynamics; shock loading; high strain rate

Citation: Luo, S.; Cui, Y. Elastodynamics Field of Non-Uniformly Moving Dislocation: From 3D to 2D. *Crystals* **2022**, *12*, 363. https://doi.org/10.3390/cryst12030363

Academic Editor: Ronald W. Armstrong

Received: 24 January 2022
Accepted: 3 March 2022
Published: 8 March 2022

1. Introduction

High strain rate deformation has long been a central concern in the fields such as machine manufacturing, automotive, aviation, aerospace, and military [1–3]. Under such loading conditions accompanied by extremely high temperature and pressure, there are many micromechanisms of plastic deformation for materials, such as dislocation and deformation twins. Complex phenomena can also arise; for example, a void can lead to high-pressure phase transformation [4], and the barrierless melt nucleation will arise for some energetic nitramine [5]. However, numerous molecular dynamics (MD) simulations have demonstrated that the dislocation density will go up with the increase of impact pressure, while the nucleation and motion of dislocations still dominate the plastic deformation of the material under the high strain rate condition [6–9]. For example, when the strain rate is below $2.77 \times 10^8/\mathrm{s}^{-1}$ and temperature is over 50 K, the plasticity is dislocation-mediated in the body-centered-cubic (BCC) metal tantalum [10]. Their simulations predict that only on reaching certain limiting conditions of stress (the uniaxial stress reaches about 8 GPa) will deformation twinning become the dominant mode of the dynamic response. Therefore, the strength and plasticity properties of a metal are dominated by dislocations in the vast majority of high strain rate deformation conditions.

According to Orowan's equation, plastic strain rate $\dot{\varepsilon} = \rho b v$ (ρ is the mobile dislocation density, b is the magnitude of Burger's vector, and v is the average dislocation velocity). If $\rho = 10^{13}/\mathrm{m}^2$, $b = 0.25$ nm, and $\dot{\varepsilon} = 5 \times 10^6/\mathrm{s}$, v is expected to be above 2 km/s, which is closed to the shear wave speed of some metals. For high-speed dislocation, its elastodynamics stress fields are significantly different from the static stress field of dislocations, which has been recognized since 1949 [11–13].

On one hand, due to the insufficient spatial and temporal resolution of experimental apparatus, it is very difficult to directly observe high-speed dislocation under such high strain rate conditions. The observation of the high-speed dislocation has extremely high requirements for laboratory equipment and samples, so far just having one report about the high-speed dislocation in a two-dimensional plasma crystal [14]. Measuring the high-speed dislocation in more materials still is very challenging and has not been successful. In order to study high-speed dislocation, most work about the 3D and 2D elastodynamics field is based on theoretical analysis, numerical calculation [15–20], and molecular dynamics simulations [21–25].

On the other hand, the underlying physics of the high-speed dislocation is substantially different from that of the quasi-static dislocations, and the high-speed dislocation is manifested in the distinctive elastodynamics field. For instance, the displacement field solution of the uniformly moving screw dislocation differs from the static solution by a "Lorentz contraction" [26]. With the increase of dislocation velocity, the stress field is contracted to the axis, perpendicular to the slip plane, on which the dislocation is located. Moreover, molecular dynamics (MD) simulations show that high-speed dislocation can enter the transonic and supersonic regimes [23,27]. Correspondingly, the special stress field of Mach cones appears [28–31]. In addition, the elastodynamics field is sensitive to the motion history of the dislocation. The elastodynamics stress fields of a uniformly expanding and shrinking dislocation loop are remarkably different, even though the final radius is both of $100b$, where b is the magnitude of Burgers vector, and its velocity magnitude is the same as $0.3c_T$ (c_T is the shear wave speed of the material) [15].

The elastodynamics effect leads to distinct dislocation interactions compared with the classical quasi-static dislocations. When the dislocations move at the low velocity, two coplanar opposite-sign colliding edge or screw dislocations annihilate. As the dislocation velocity increases close to the shear wave speed, those two dislocations, moving against each other, fully overshoot each other, even generating new dislocations on near planes [22,24,32]. In addition, the annihilation of a dislocation from the free surface is generally observed when it moves with a low velocity. Unexpectedly, the rebounding of a edge or a screw dislocation from the free surface has been found when it moves at a high-velocity [33]. These abnormal mechanisms can lead to a rapid increase in dislocation density that is strongly correlated both spatially and temporally, affecting high-strain-rate plastic deformation from the microscopic level. However, to this day, the elastodynamics effect on high-speed dislocation is far from being well understood, because the full history-dependent nature and spatial–temporal coupling feature significantly complicate the analysis of the problem.

Among the elastodynamics effect on high-speed dislocation, a fundamental problem is that the elastodynamics solution of high-speed dislocation looks very different for two-dimensional (2D) and three-dimensional (3D) cases. Most previous focus has been put on the 2D infinitely long straight pure screw or edge high-speed dislocations [20,31,34]. For 2D screw dislocation, it is derived based on the assumption of anti-plane strain framework, and for 2D edge dislocation, it is derived based on the plane strain framework. For the 3D case, a general theory of non-singular dislocations loop is also developed for homogeneous and isotropic infinite material [15,35]. After the concept of dislocation appeared, the theory of quasi-static dislocations has been well developed [26]. The stress fields of the high-speed dislocation are substantially different from those of the quasi-static dislocations, which have been reported since 1949 [11,12]. From then on, dislocation elastodynamics theories were further developed [13]. In the last ten years, the fundamental time-dependent solutions for the injection and non-uniform motion of straight edge and screw dislocations are widely studied. The two-dimensional elastodynamics Green tensor is used to obtain the elastodynamics field of the subsonic, transonic, or supersonic dislocation motion [20]. Refs. [13,31] have made several important contributions for elastodynamics solutions for the non-uniform motion of 3D dislocations. To complete the 3D elastodynamics framework, Cui et al. have built explicit compact formula of high-speed 3D dislocations with non-

uniform motion, which can be directly used for the numerical implementation [15]. The corresponding mathematical formula of the stress fields of three-dimensional (3D) and two-dimensional (2D) dislocations looks quite different (see Equations (9), (10), and (16), which will be discussed in detail later).

However, few scholars have paid attention to the connection and physical differences between the 3D and 2D of non-uniformly moving dislocation's elastodynamics field, even though it is important to connect the 2D and 3D underlying mechanisms. To our knowledge, only for quasi-static dislocation, Lazar built up the 2D elastic fields from 3D elastostatics solution for anisotropic elasticity in Fourier space [36]. However, for high-speed dislocation, how to directly obtain the 2D solution from the 3D elastodynamics solution is seldomly discussed. In the present work, 3D and 2D elastodynamics Green tensors act as mediums for correlations between both elastodynamics fields, the 2D dislocation elastodynamics is successfully derived from the higher dimensional elastodynamics fields, and their intrinsic physical connections and distinctions are investigated.

2. Eastodynamics Solution of Non-Uniformly Moving Dislocation

The elastodynamics stress field of a 3D non-uniformly moving dislocation loop is as follows:

$$\begin{aligned}\sigma_{ij}(\mathbf{x},t) &= C_{ijkl}\beta^E_{kl}(\mathbf{x},t)\\ &= \int_{t_0}^{t} \mathrm{d}t' \oint_{\mathcal{L}(t')} \epsilon_{rql} C_{ijkl} C_{mnpq} G_{km,n}(\mathbf{x}-\mathbf{x}',t-t') b_p \xi_r(\mathbf{x}',t') \mathrm{d}L'\\ &- \int_{t_0}^{t} \mathrm{d}t' \oint_{\mathcal{L}(t')} C_{ijkl}\rho \dot{G}_{kp}(\mathbf{x}-\mathbf{x}',t-t') b_p \epsilon_{lsr} V_s(\mathbf{x}',t') \xi_r(\mathbf{x}',t') \mathrm{d}L'\end{aligned} \tag{1}$$

where C_{ijkl} is the elastic modulus tensor, β^E_{kl} is the elastic distortion solution, ρ is the material density, G_{kp} is the elastodynamics Green tensor at the 3D, the subscript using Greek alphabet ranges from 1 to 3 for 3D case. $()_{,n}$ denotes differentiation with respect to x_n. A superposed dot means a time derivative. t_0 and t represent the initial and current time, $\mathbf{x}$ is a position vector of the observer point. $\mathbf{x}'$ is the integration point position at time t' along the dislocation line $\mathcal{L}$. $\mathbf{b}$ is the Burgers vector, $\mathbf{V}$ is the dislocation velocity vector, and ξ is the unit tangent direction vector of the dislocation line. The deriviation of Equation (1) is referred to [13,15,37–39].

Equation (1) clearly show that the elastodynamics solution is spatial–temporal coupled and depends on the full history of the dislocation motion. In order to obtain the 3D and 2D solution in the same framework, the first key problem is to obtain the corresponding elastodynamics Green tensor and its degradation for 2D problems.

3. Degradation of Elastodynamics Green Tensor

This section will demonstrate how to degrade the 3D elastodynamics Green tensor to the 2D counterpart, corresponding to the problems of infinitely long straight dislocation lines.

The 3D elastodynamics Green's function in an isotropic crystal is derived in [40,41],

$$\begin{aligned}G_{ij}(\mathbf{x},t) = \frac{-1}{4\pi\rho x}\Bigg\{ &\frac{1}{c_T^2}\left(\delta_{ij}-\frac{x_i x_j}{x^2}\right)\delta\left(t-\frac{x}{c_T}\right) + \frac{1}{c_L^2}\frac{x_i x_j}{x^2}\delta\left(t-\frac{x}{c_L}\right)\\ &+\left(\frac{3x_i x_j}{x^2}-\delta_{ij}\right)\frac{1}{x^2}\int_{x/c_L}^{x/c_T}\tau\delta(t-\tau)d\tau\Bigg\}\end{aligned} \tag{2}$$

where x and x_i represent the magnitude and the ith component of vector $\mathbf{x}$, respectively. δ_{ij} is the Kronecker delta. c_T and c_L are the transverse and longitudinal wave speed, respectively.

Without loss of generality, an infinite-long straight dislocation is assumed to be along the x_3 direction (see Figure 1a). Therefore, the degradation of elastodynamics Green tensor

needs to integrate Equation (2) for x_3 from $-\infty$ to ∞. c is used to express a specific elastic wave velocity c, which may be c_{T}, c_{L}, or the elastic wave speed between c_{T} and c_{L}. Then, the basic term in Equation (2) can be expressed as $f(\mathbf{x},t)\delta\left(t-\frac{x}{c}\right)$. Its integration can be calculated as follows,

$$\int_{-\infty}^{\infty} f(\mathbf{x},t)\delta\left(t-\frac{x}{c}\right)dx_3 = \frac{f(\mathbf{x},t)}{\frac{1}{c}\frac{dx}{dx_3}}|_{x=ct} = \frac{2f(\mathbf{x},t)}{\frac{1}{c}\frac{x_3}{x}}|_{x=ct} = \frac{2ctf(\mathbf{x},t)}{\sqrt{t^2-l^2/c^2}}|_{x=ct} \tag{3}$$

where $l^2 = x_1^2 + x_2^2$. According to Equation (3), many basic equations can be obtained to calculate the 2D elastodynamics Green tensor and its time derivative, as listed in Appendix A. Combining Appendix A and Equation (2), the 2D elastodynamics Green tensor becomes,

$$\begin{aligned} G_{\alpha\beta}(\mathbf{x},t) =& \frac{-1}{2\pi\rho}\left\{\frac{\delta_{\alpha\beta}}{l^2}\left(\frac{t^2H(t^2-l^2/c_T^2)}{\sqrt{t^2-l^2/c_T^2}} - \sqrt{t^2-l^2/c_L^2}H(t^2-l^2/c_L^2)\right)\right. \\ &\left. + \frac{x_\alpha x_\beta}{l^4}\left(\frac{(-2t^2+l^2/c_T^2)H(t^2-l^2/c_T^2)}{\sqrt{t^2-l^2/c_T^2}} + \frac{(2t^2-l^2/c_L^2)H(t^2-l^2/c_L^2)}{\sqrt{t^2-l^2/c_L^2}}\right)\right\} \end{aligned} \tag{4}$$

$$G_{33}(\mathbf{x},t) = \frac{-1}{2\pi\mu\sqrt{t^2-l^2/c_T^2}} \tag{5}$$

$$G_{\alpha 3}(\mathbf{x},t) = 0 \tag{6}$$

where the Roman subscripts α and β range from 1 to 2.

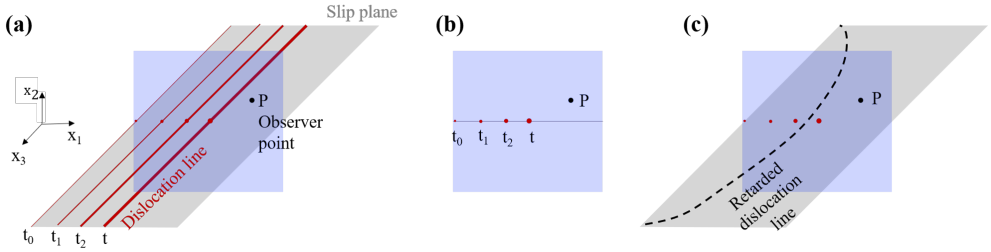

Figure 1. (**a**) Schematic showing a high-speed infinite-long straight dislocation line; (**b**) Schematic showing the integration strategy of a 2D dislocation line; (**c**) Schematic showing the integration strategy based on retarded dislocation.

For isotropic material, $C_{ijkl} = \lambda\delta_{ij}\delta_{kl} + \mu(\delta_{ik}\delta_{jl} + \delta_{il}\delta_{jk})$, where λ and μ are Lamé's first parameter and shear modulus, respectively. According to Equation (1),

$$\begin{aligned} \beta_{kl}^{\mathrm{E}}(\mathbf{x},t) =& \int_{t_0}^{t} \mathrm{d}t' \oint_{\mathcal{L}(t')} [\lambda\epsilon_{rql}G_{km,m}(-\mathbf{s}',t-t')b_q\xi_r(\mathbf{s}',t') \\ &+ \mu\epsilon_{rql}G_{kp,q}(-\mathbf{s}',t-t')b_p\xi_r(\mathbf{s}',t') + \mu\epsilon_{rql}G_{kq,p}(-\mathbf{s}',t-t')b_p\xi_r(\mathbf{s}',t')]\mathrm{d}L' \\ &- \int_{t_0}^{t} \mathrm{d}t' \oint_{\mathcal{L}(t')} \rho\dot{G}_{kp}(-\mathbf{s}',t-t')b_p\epsilon_{lsr}V_s(\mathbf{s}',t')\xi_r(\mathbf{s}',t')\mathrm{d}L'. \end{aligned} \tag{7}$$

For screw dislocation, the dislocation line vector $\xi = [001]$, so the Burger vector $\mathbf{b} = [00b]$. It is easy to see from Equation (7) that $\epsilon_{rql}b_q\xi_r = 0$, so only $G_{k3,p}$, $G_{kp,3}$, and $\dot{G}_{k3,t}$ contribute. Since $G_{\alpha\beta},3 = 0$, $G_{\alpha 3} = 0$, only G_{33} plays a role.

With respect to edge dislocation, the dislocation line vector $\xi = [001]$, and the Burger vector $\mathbf{b} = [b00]$. According to Equation (7), only $G_{km,m}$, $G_{k1,q}$, $G_{kq,1}$, and $\dot{G}_{k1}$ contribute, where subscript q cannot be 3. Since $G_{31} = 0$, $G_{\alpha 3} = 0$, and $G_{33,3} = 0$, only $G_{\alpha\beta}$ plays a role.

The obtained 2D Green tensor is consistent with previous work, which is derived for a plane-strain and anti-plane strain problem with respect to edge dislocation and screw dislocation, respectively [31].

4. Different Spatial–Temporal Decoupling Strategies at 2D and 3D

4.1. Spatial–Temporal Decoupling Strategy at 2D

The degradation of elastodynamics Green tensor indicates that for an infinitely long straight dislocation in infinitely extended material, the spatial–temporal coupling integration is firstly done on a spatial scale, because the geometry of the dislocation line remains unchanged, as indicated by the dislocation configuration at different times (t_0, t_1, t_2, t) in Figure 1a. When the dislocations are assumed to be always straight, along x_3 all the time, the intersection point of the dislocation line and plane Ox_1x_2 can well describe the position of dislocation at different times. The straight line integrals along the dislocation are clear and definite at any time. Depending on the atomic displacement caused by the screw and edge dislocation, it will be the anti-plane strain problem of screw dislocation and plane strain problem of edge dislocation. Therefore, the 2D treatment is able to represent the 3D information of the infinitely long straight dislocation, which is similar to previous work, such as [17,31]. Afterward, this problem can be simplified as a 2D problem. As described in Figure 1b, each infinite long straight dislocation line is represented through a point, which is marked by the red nodes at different times. Then, only time integration is required to obtain the elastodynamics solution.

As discussed in Section 3, for screw dislocation, only G_{33} works. The time derivative of G_{33} is,

$$\begin{aligned}\dot{G}_{33}(\mathbf{x}-\mathbf{x}',t-t') &= \frac{\partial G_{33}(\mathbf{x}-\mathbf{x}',t-t')}{\partial t'} + \frac{\partial G_{33}(\mathbf{x}-\mathbf{x}',t-t')}{\partial x'_\eta}\frac{\partial x'_\eta}{\partial t'} \\ &= -G_{33,t'}(\mathbf{x}-\mathbf{x}',t-t') - G_{33,\eta}(\mathbf{x}-\mathbf{x}',t-t')V_\eta \\ &= \frac{\widetilde{t}H(\widetilde{t}^2 - l^2/c_T^2)}{2\pi\mu\sqrt{(\widetilde{t}^2 - l^2/c_T^2)^3}} - \frac{(x_\eta - x'_\eta)H(\widetilde{t}^2 - l^2/c_T^2)}{2\pi c_T^2\mu\sqrt{(\widetilde{t}^2 - l^2/c_T^2)^3}}V_\eta\end{aligned} \tag{8}$$

where $\widetilde{t} = t - t'$, $l^2 = (x_1 - x'_1)^2 + (x_2 - x'_2)^2$, $\eta = 1, 2$, $G_{33}|_{t'=t} = 0$, $V_k|_{t'=0} = 0$. Combining Equations (7) and (8), we can obtain the strain field function of non-uniformly moving screw dislocation,

$$
\begin{aligned}
\beta_{31}^{E} &= \int_0^t [\mu G_{33,2}(\mathbf{x}-\mathbf{x}',t-t')b_3\xi_3 + \rho\dot{G}_{33}(\mathbf{x}-\mathbf{x}',t-t')V_2 b_3\xi_3]dt' \\
&= \int_0^t \left[\mu G_{33,2}(\mathbf{x}-\mathbf{x}',t-t')b_3\xi_3 - \mu G_{33,\eta}(\mathbf{x}-\mathbf{x}',t-t')\frac{V_\eta}{c_T^2}V_2 b_3\xi_3\right]dt' \\
&\quad - \int_0^t \rho G_{33,t'}(\mathbf{x}-\mathbf{x}',t-t')V_2 b_3\xi_3 dt' \\
&= \int_0^t \left[\mu G_{33,2}(\mathbf{x}-\mathbf{x}',t-t')b_3\xi_3 - \mu G_{33,\eta}(\mathbf{x}-\mathbf{x}',t-t')\frac{V_\eta}{c_T^2}V_2 b_3\xi_3\right]dt' \\
&\quad + \int_0^t \rho G_{33}(\mathbf{x}-\mathbf{x}',t-t')\dot{V}_2 b_3\xi_3 dt' \\
&\quad - \rho G_{33}(\mathbf{x}-\mathbf{x}',t-t')V_2 b_3\xi_3|_{t'=0}^{t'=t} \\
&= \int_0^t \left[\mu G_{33,2}(\mathbf{x}-\mathbf{x}',t-t')b_3\xi_3 - \mu G_{33,\eta}(\mathbf{x}-\mathbf{x}',t-t')\frac{V_\eta}{c_T^2}V_2 b_3\xi_3\right]dt' \\
&\quad + \int_0^t \rho G_{33}(\mathbf{x}-\mathbf{x}',t-t')\dot{V}_2 b_3\xi_3 dt' \\
&= \int_0^t \left[\mu G_{33,2}(\mathbf{x}-\mathbf{x}',t-t')b_3\xi_3 - \mu G_{33,1}(\mathbf{x}-\mathbf{x}',t-t')\frac{V_1}{c_T^2}V_2 b_3\xi_3\right. \\
&\quad \left. -\mu G_{33,2}(\mathbf{x}-\mathbf{x}',t-t')\frac{V_2}{c_T^2}V_2 b_3\xi_3\right]dt' + \int_0^t \rho G_{33}(\mathbf{x}-\mathbf{x}',t-t')\dot{V}_2 b_3\xi_3 dt' \\
&= \frac{b_3\xi_3}{2\pi c_T^2}\int_0^t \left[\frac{\dot{V}_2}{\sqrt{\tilde{t}^2 - l^2/c_T^2}} + \left(1-\frac{V_2^2}{c_T^2}\right)\frac{(x_2-x_2')}{\sqrt{(\tilde{t}^2 - l^2/c_T^2)^3}}\right. \\
&\quad \left. -\frac{V_1V_2}{c_T^2}\frac{(x_1-x_1')}{\sqrt{(\tilde{t}^2 - l^2/c_T^2)^3}}\right]H(\tilde{t}^2 - l^2/c_T^2)dt'
\end{aligned} \tag{9}
$$

$$
\begin{aligned}
\beta_{32}^{E} &= -\int_0^t [\mu G_{33,1}(\mathbf{x}-\mathbf{x}',t-t')b_3\xi_3 + \rho\dot{G}_{33}(\mathbf{x}-\mathbf{x}',t-t')V_1 b_3\xi_3]dt' \\
&= -\frac{b_3\xi_3}{2\pi c_T^2}\int_0^t \left[\frac{\dot{V}_1}{\sqrt{\tilde{t}^2 - l^2/c_T^2}} + \left(1-\frac{V_1^2}{c_T^2}\right)\frac{(x_1-x_1')}{\sqrt{(\tilde{t}^2 - l^2/c_T^2)^3}}\right. \\
&\quad \left. -\frac{V_1V_2}{c_T^2}\frac{(x_2-x_2')}{\sqrt{(\tilde{t}^2 - l^2/c_T^2)^3}}\right]H(\tilde{t}^2 - l^2/c_T^2)dt'
\end{aligned} \tag{10}
$$

$$
\beta_{11}^{E} = \beta_{12}^{E} = \beta_{13}^{E} = \beta_{21}^{E} = \beta_{22}^{E} = \beta_{23}^{E} = \beta_{33}^{E} = 0 \tag{11}
$$

For screw dislocation considered with constant speed V, at time $t = 0.15$ ns, the numerical results of Equations (9) and (10) can be seen in Figure 2. The 2D elastodynamics stress fields derived from the degradation of 3D are consistent with 3D-discrete dislocation elastodynamics solutions in [15].

For edge dislocation, we can obtain,

$$
\dot{G}_{\alpha\beta}(\mathbf{x}-\mathbf{x}',t-t') = -G_{\alpha\beta,t'}(\mathbf{x}-\mathbf{x}',t-t') - G_{\alpha\beta,\gamma}(\mathbf{x}-\mathbf{x}',t-t')V_\gamma \tag{12}
$$

where $\alpha, \beta, \gamma = 1, 2$, $G_{\alpha\beta}|_{t'=t} = 0$, $V_\gamma|_{t'=0} = 0$.

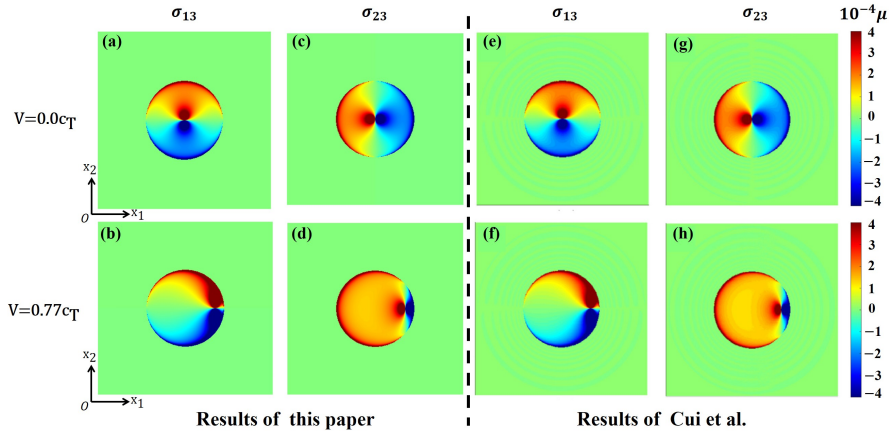

Figure 2. Stress field of screw dislocation with $V = 0$ or $0.77c_T$, at $t = 0.15$ ns in the $0x_1x_2$ plane (μ is the shear model of the material). (**a**–**d**) Two-dimensional (2D) elastodynamics solution by Equations (9) and (10), (**e**–**h**) 3D elastodynamics field in [15].

According to Equation (4), the derivative of $\sqrt{t^2 - l^2/c^2}$ is given by,

$$\left(\sqrt{t^2 - l^2/c^2}\right)_{,\gamma} = -\frac{l}{c^2\sqrt{t^2 - l^2/c^2}}\frac{\partial l}{\partial x_\gamma}H(t^2 - l^2/c^2) = -\frac{x_\gamma}{c^2\sqrt{t^2 - l^2/c^2}}H(t^2 - l^2/c^2) \tag{13}$$

The derivative of $\dfrac{1}{l^m\sqrt{t^2 - l^2/c^2}}$ is,

$$\left(\frac{1}{l^m\sqrt{t^2 - l^2/c^2}}\right)_{,\gamma} = -\frac{mx_\gamma H(t^2 - l^2/c^2)}{l^{m+2}\sqrt{t^2 - l^2/c^2}} + \frac{x_\gamma H(t^2 - l^2/c^2)}{c^2 l^m\sqrt{(t^2 - l^2/c^2)^3}} \tag{14}$$

where $m \geqslant 0$, $c = c_T, c_L$. Using Equations (13) and (14) and $\partial x_\alpha/\partial x_\gamma = \delta_{\alpha\gamma}$, the derivative of the 2D Green function is expressed as

$$\begin{aligned}
G_{\alpha\beta,\gamma}(\mathbf{x},t) = \frac{1}{2\pi\rho}\Bigg\{ & \left(\frac{\delta_{\alpha\gamma}x_\beta + \delta_{\beta\gamma}x_\alpha}{l^4} - \frac{4x_\alpha x_\beta x_\gamma}{l^6}\right)\left[\left(\frac{t^2}{\sqrt{t^2 - l^2/c_L^2}} + \sqrt{t^2 - l^2/c_L^2}\right)H(t^2 - l^2/c_L^2)\right. \\
& \left. - \left(\frac{t^2}{\sqrt{t^2 - l^2/c_T^2}} + \sqrt{t^2 - l^2/c_T^2}\right)H(t^2 - l^2/c_T^2)\right] \\
& + \frac{x_\alpha x_\beta x_\gamma}{l^4}\left[\frac{t^2/c_L^2 H(t^2 - l^2/c_L^2)}{\sqrt{(t^2 - l^2/c_L^2)^3}} - \frac{H(t^2 - l^2/c_L^2)}{c_L^2\sqrt{t^2 - l^2/c_L^2}}\right. \\
& \left. - \frac{t^2/c_T^2 H(t^2 - l^2/c_T^2)}{\sqrt{(t^2 - l^2/c_T^2)^3}} + \frac{H(t^2 - l^2/c_T^2)}{c_T^2\sqrt{t^2 - l^2/c_T^2}}\right] \\
& + \frac{2\delta_{\alpha\beta}x_\gamma}{l^4}\left[\sqrt{t^2 - l^2/c_L^2}H(t^2 - l^2/c_L^2) - \frac{t^2 H(t^2 - l^2/c_T^2)}{\sqrt{t^2 - l^2/c_T^2}}\right] \\
& + \frac{\delta_{\alpha\beta}x_\gamma}{l^2}\left[\frac{H(t^2 - l^2/c_L^2)}{c_L^2\sqrt{t^2 - l^2/c_L^2}} + \frac{t^2 H(t^2 - l^2/c_T^2)}{c_T^2\sqrt{(t^2 - l^2/c_T^2)^3}}\right]\Bigg\}
\end{aligned} \tag{15}$$

Substituting Equations (12) and (15) into Equation (7), we can obtain the elastodynamics field of non-uniformly moving edge dislocation,

$$
\begin{aligned}
\beta^E_{\alpha\iota} &= \int_0^t \left[\epsilon_{n\varsigma\iota} G_{\alpha\beta,\gamma}(\mathbf{x}-\mathbf{x}',t-t') C_{\beta\gamma\kappa\varsigma}(\mathbf{t}') b_\kappa \xi_n - \epsilon_{\iota\varsigma n}\rho \dot{G}_{\alpha\beta}(\mathbf{x}-\mathbf{x}',t-t') V_\varsigma b_\beta \xi_n\right] dt' \\
&= \int_0^t \epsilon_{n\varsigma\iota}\left[G_{\alpha\beta,\gamma}(\mathbf{x}-\mathbf{x}',t-t') C_{\beta\gamma\kappa\varsigma}(\mathbf{t}') b_\kappa \xi_n + \rho \dot{G}_{\alpha\beta}(\mathbf{x}-\mathbf{x}',t-t') V_\varsigma b_\beta \xi_n\right] dt' \\
&= \int_0^t \epsilon_{n\varsigma\iota}\Big[G_{\alpha\beta,\gamma}(\mathbf{x}-\mathbf{x}',t-t')(C_{\beta\gamma\kappa\varsigma} - \rho V_\gamma V_\varsigma \delta_{\beta\kappa}) b_\kappa \xi_n - \rho G_{\alpha\beta,t'}(\mathbf{x}-\mathbf{x}',t-t') V_\varsigma b_\beta \xi_n\Big] dt' \\
&= \int_0^t \epsilon_{n\varsigma\iota}\left[G_{\alpha\beta,\gamma}(\mathbf{x}-\mathbf{x}',t-t')(C_{\beta\gamma\kappa\varsigma} - \rho V_\gamma V_\varsigma \delta_{\beta\kappa}) b_\kappa \xi_n + \rho G_{\alpha\beta}(\mathbf{x}-\mathbf{x}',t-t') \dot{V}_\varsigma b_\beta \xi_n\right] dt' \\
&\quad - \epsilon_{n\varsigma\iota}\rho G_{\alpha\beta}(\mathbf{x}-\mathbf{x}',t-t') V_\varsigma b_\beta \xi_n|_{t'=0}^{t'=t} \\
&= \int_0^t \epsilon_{n\varsigma\iota}\left[G_{\alpha\beta,\gamma}(\mathbf{x}-\mathbf{x}',t-t')(C_{\beta\gamma\kappa\varsigma} - \rho V_\gamma V_\varsigma \delta_{\beta\kappa}) b_\kappa \xi_n + \rho G_{\alpha\beta}(\mathbf{x}-\mathbf{x}',t-t') \dot{V}_\varsigma b_\beta \xi_n\right] dt' \\
&= \frac{1}{2\pi\rho}\int_0^t \Bigg\{ \left(\frac{\delta_{\alpha\gamma}\widetilde{x_\beta} + \delta_{\beta\gamma}\widetilde{x_\alpha}}{l^4} - \frac{4\widetilde{x_\alpha}\widetilde{x_\beta}\widetilde{x_\gamma}}{l^6}\right)\left[\left(\frac{\widetilde{t}^2}{\sqrt{\widetilde{t}^2 - l^2/c_T^2}} + \sqrt{\widetilde{t}^2 - l^2/c_T^2}\right) H(\widetilde{t}^2 - l^2/c_T^2)\right. \\
&\quad \left. - \left(\frac{\widetilde{t}^2}{\sqrt{\widetilde{t}^2 - l^2/c_L^2}} + \sqrt{\widetilde{t}^2 - l^2/c_L^2}\right) H(\widetilde{t}^2 - l^2/c_L^2)\right] \\
&\quad + \frac{\widetilde{x_\alpha}\widetilde{x_\beta}\widetilde{x_\gamma}}{l^4}\left[\frac{\widetilde{t}^2/c_L^2 H(\widetilde{t}^2 - l^2/c_L^2)}{\sqrt{(\widetilde{t}^2 - l^2/c_L^2)^3}} - \frac{H(\widetilde{t}^2 - l^2/c_L^2)}{c_L^2\sqrt{\widetilde{t}^2 - l^2/c_L^2}} - \frac{\widetilde{t}^2/c_T^2 H(\widetilde{t}^2 - l^2/c_T^2)}{\sqrt{(\widetilde{t}^2 - l^2/c_T^2)^3}} + \frac{H(\widetilde{t}^2 - l^2/c_T^2)}{c_T^2\sqrt{\widetilde{t}^2 - l^2/c_L^2}}\right] \\
&\quad + \frac{2\delta_{\alpha\beta}\widetilde{x_\gamma}}{l^4}\left[\sqrt{\widetilde{t}^2 - l^2/c_L^2} H(\widetilde{t}^2 - l^2/c_L^2) - \frac{\widetilde{t}^2 H(\widetilde{t}^2 - l^2/c_T^2)}{\sqrt{\widetilde{t}^2 - l^2/c_T^2}}\right] \\
&\quad + \frac{\delta_{\alpha\beta}\widetilde{x_\gamma}}{l^2}\left[\frac{H(\widetilde{t}^2 - l^2/c_L^2)}{c_L^2\sqrt{\widetilde{t}^2 - l^2/c_L^2}} + \frac{\widetilde{t}^2 H(\widetilde{t}^2 - l^2/c_T^2)}{c_T^2\sqrt{(t^2 - l^2/c_T^2)^3}}\right]\Bigg\} \epsilon_{n\varsigma\iota}(C_{\beta\gamma\kappa\varsigma} - \rho V_\gamma V_\varsigma \delta_{\beta\kappa}) b_\kappa \xi_n dt' \\
&\quad + \rho\Bigg\{\frac{\delta_{\alpha\beta}}{l^2}\left(\frac{\widetilde{t}^2 H(\widetilde{t}^2 - l^2/c_T^2)}{\sqrt{\widetilde{t}^2 - l^2/c_T^2}} - \sqrt{\widetilde{t}^2 - l^2/c_L^2} H(\widetilde{t}^2 - l^2/c_L^2)\right) \\
&\quad + \frac{\widetilde{x_\alpha}\widetilde{x_\beta}}{l^4}\left(\frac{(-2\widetilde{t}^2 + l^2/c_T^2) H(\widetilde{t}^2 - l^2/c_T^2)}{\sqrt{\widetilde{t}^2 - l^2/c_T^2}} + \frac{(2\widetilde{t}^2 - l^2/c_L^2) H(\widetilde{t}^2 - l^2/c_L^2)}{\sqrt{\widetilde{t}^2 - l^2/c_L^2}}\right)\Bigg\} \epsilon_{n\varsigma\iota} \dot{V}_\varsigma b_\beta \xi_n dt'
\end{aligned}
\tag{16}
$$

where $\widetilde{t} = t - t'$, $\widetilde{x_\alpha} = x_\alpha - x'_\alpha (\alpha = 1, 2)$, $l^2 = \widetilde{x_1}^2 + \widetilde{x_2}^2$. The 2D elastodynamics results of Equations (9), (10), and (16) are in agreement with the previous works [31].

4.2. Spatial–Temporal Decoupling Strategy at 3D

However, the spatial–temporal decoupling strategies at 2D dislocation discussed above are not applied to arbitrarily moving 3D dislocation, because their 3D geometry and curvature keep changing during plastic deformation. Therefore, the alternative strategy is to carry out the temporal integration firstly. As a result of the existence of the Dirac delta function $\delta(t - t' - \frac{x - x'}{c})$ in Green's function, the retarded solution used in Equation (1) is obtained as follows by performing temporal integration.

$$
\mathcal{L}(t - R/c) = \left\{\mathbf{x}' \text{ such that } \|\mathbf{x} - \mathbf{x}'(t_{\text{ret}})\| = c(t - t_{\text{ret}})\right\} \tag{17}
$$

where $\mathbf{x}'$ is a source position on the retarded dislocation and $\mathcal{L}(t - R/c)$ represents the collection of retarded points $\mathbf{x}'$ on an arbitrarily moving 3D dislocation. $\mathbf{x}$ is the observer point. t_{ret} is retarded time corresponding to a specific elastic wave velocity c. For retarded dislocation, we make use of a simple example of subsonic 3D dislocation, sliding in plane Ox_1x_3, with constant velocity V to elaborate the case. For retarded dislocation, we make use

of a simple example of subsonic 3D dislocation, sliding in plane Ox_1x_3 with constant speed V. As shown in Figure 1c, for the arbitrary observer point P $(x_1^P, x_2^P, 0)$ in plane Ox_1x_2, after the temporal integration, the points $(Vt_r, 0, x_3^r)$ on the retarded dislocation line satisfy $(x_1^P - Vt_r)^2 + (x_2^P)^2 + (x_3^B)^2 = c_T^2(t - t_r)^2$, where t_r is the retarded time corresponding to the shear wave (c_T). More examples of retarded dislocations can be seen in [15]. For 3D moving dislocation with arbitrary curve configuration, complex curve integrals along the retarded dislocation contain the 3D space information of elastodynamics fields.

This technique of using retarded potentials simplifies the calculation of coupled spatial and temporal integration to a spatial integral over retarded dislocation positions. This retarded potential method is standard in electrodynamics [42]. This method extends the technique of retarded potentials, which was originally used to describe the electrodynamics of charged particles moving near the speed of light. The retarded functions are the consequence of the finite speed of the wave and with respect to the effect of retardation. This idea is applicable to any dynamical theory with retardation, including elastodynamics [39]. The simplest example is the well-known Doppler effect in acoustics.

Accordingly, the elastodynamics stress field of arbitrarily moving 3D dislocation is as follows [15],

$$\boldsymbol{\text{œ}}(\mathbf{x}, t) = \frac{\mu}{4\pi}\Big(\mathbf{s}(\mathbf{x}, t) + \mathbf{s}^{\mathrm{T}}(\mathbf{x}, t)\Big), \tag{18}$$

where the auxiliary tensor $\mathbf{s}(\mathbf{x}, t)$ is given by,

$$\begin{aligned}
\mathbf{s}(\mathbf{x},t) = {} & \oint_{\mathcal{L}(t-R/c_T)} \frac{1}{R^2(R-\mathbf{R}\cdot\mathbf{V}/c_T)}\Bigg(-2\mathbf{R}\otimes(\mathbf{b}\times) + \frac{-\nu}{1-2\nu}\mathbf{b}\cdot(\mathbf{R}\times)\mathbf{I} \\
& -3\Bigg(\mathbf{b} - 4\frac{\mathbf{R}\cdot\mathbf{b}}{R^2}\mathbf{R}\Bigg)\otimes(\mathbf{R}\times)\Bigg)\mathrm{d}L' \\
& - \partial_t \oint_{\mathcal{L}(t-R/c_T)} \frac{1}{c_T R(R-\mathbf{R}\cdot\mathbf{V}/c_T)}\Bigg(\frac{\nu}{1-2\nu}\mathbf{b}\cdot(\mathbf{R}\times)\mathbf{I} + \Bigg(\mathbf{b} - \frac{2\mathbf{R}\cdot\mathbf{b}}{R^2}\mathbf{R}\Bigg)\otimes(\mathbf{R}\times)\Bigg)\mathrm{d}L' \\
& + \oint_{\mathcal{L}(t-R/c_L)} \frac{1-2\nu}{(1-\nu)R^2(R-\mathbf{R}\cdot\mathbf{V}/c_L)}\Bigg(\frac{1-3\nu}{1-2\nu}\mathbf{R}\otimes(\mathbf{b}\times) + \frac{\nu^2}{(1-2\nu)^2}\mathbf{b}\cdot(\mathbf{R}\times)\mathbf{I} \\
& + \Bigg(\mathbf{b} - \frac{6\mathbf{R}\cdot\mathbf{b}}{R^2}\mathbf{R}\Bigg)\otimes(\mathbf{R}\times)\Bigg)\mathrm{d}L' \\
& - \partial_t \oint_{\mathcal{L}(t-R/c_L)} \frac{1-2\nu}{(1-\nu)c_L R(R-\mathbf{R}\cdot\mathbf{V}/c_L)}\Bigg(\frac{\nu}{1-2\nu}\mathbf{R}\otimes(\mathbf{b}\times) - \frac{\nu^2}{(1-2\nu)^2}\mathbf{b}\cdot(\mathbf{R}\times)\mathbf{I} \\
& + \Bigg(\quad \frac{\mathbf{R}\cdot\mathbf{b}}{R^2}\mathbf{R}\Bigg)\otimes(\mathbf{R}\times)\Bigg)\mathrm{d}L' \\
& + \int_{1/c_L}^{1/c_T}\oint_{\mathcal{L}(t-R\kappa)} \frac{6c_T^2\kappa}{R^2(R-\mathbf{R}\cdot\mathbf{V}\kappa)}\Bigg(\mathbf{R}\otimes(\mathbf{b}\times) \quad + \Bigg(\mathbf{b} - \frac{5\mathbf{R}\cdot\mathbf{b}}{R^2}\mathbf{R}\Bigg)\otimes(\mathbf{R}\times)\Bigg)\mathrm{d}L'\mathrm{d}\kappa \\
& + \partial_t \oint_{\mathcal{L}(t-R/c_T)} \frac{1}{c_T^2(R-\mathbf{R}\cdot\mathbf{V}/c_T)}\Bigg(\frac{\nu}{1-2\nu}\Bigg(\mathbf{b} - \frac{\mathbf{R}\cdot\mathbf{b}}{R^2}\mathbf{R}\Bigg)\cdot(\mathbf{V}\times)\mathbf{I} + \Bigg(\mathbf{b} - \frac{\mathbf{R}\cdot\mathbf{b}}{R^2}\mathbf{R}\Bigg)\otimes(\mathbf{V}\times)\Bigg)\mathrm{d}L' \\
& + \partial_t \oint_{\mathcal{L}(t-R/c_L)} \frac{1}{c_L^2(R-\mathbf{R}\cdot\mathbf{V}/c_L)}\Bigg(\frac{\nu}{1-2\nu}\Bigg(\quad \frac{\mathbf{R}\cdot\mathbf{b}}{R^2}\mathbf{R}\Bigg)\cdot(\mathbf{V}\times)\mathbf{I} + \Bigg(\quad \frac{\mathbf{R}\cdot\mathbf{b}}{R^2}\mathbf{R}\Bigg)\otimes(\mathbf{V}\times)\Bigg)\mathrm{d}L' \\
& - \int_{1/c_L}^{1/c_T}\oint_{\mathcal{L}(t-R\kappa)} \frac{1}{R(R-\mathbf{R}\cdot\mathbf{V}\kappa)}\Bigg(\frac{\nu}{1-2\nu}\Bigg(\mathbf{b} - \frac{3\mathbf{R}\cdot\mathbf{b}}{R^2}\mathbf{R}\Bigg)\cdot(\mathbf{V}\times)\mathbf{I} + \Bigg(\mathbf{b} - \frac{3\mathbf{R}\cdot\mathbf{b}}{R^2}\mathbf{R}\Bigg)\otimes(\mathbf{V}\times)\Bigg)\mathrm{d}L'\mathrm{d}\kappa \\
& + \oint_{\mathcal{L}(t-R/c_T)} \frac{1}{c_T R(R-\mathbf{R}\cdot\mathbf{V}/c_T)}\Bigg(\frac{\nu}{1-2\nu}\Bigg(\mathbf{b} - \frac{3\mathbf{R}\cdot\mathbf{b}}{R^2}\mathbf{R}\Bigg)\cdot(\mathbf{V}\times)\mathbf{I} + \Bigg(\mathbf{b} - \frac{3\mathbf{R}\cdot\mathbf{b}}{R^2}\mathbf{R}\Bigg)\otimes(\mathbf{V}\times)\Bigg)\mathrm{d}L' \\
& - \oint_{\mathcal{L}(t-R/c_L)} \frac{1}{c_L R(R-\mathbf{R}\cdot\mathbf{V}/c_L)}\Bigg(\frac{\nu}{1-2\nu}\Bigg(\mathbf{b} - \frac{3\mathbf{R}\cdot\mathbf{b}}{R^2}\mathbf{R}\Bigg)\cdot(\mathbf{V}\times)\mathbf{I} + \Bigg(\mathbf{b} - \frac{3\mathbf{R}\cdot\mathbf{b}}{R^2}\mathbf{R}\Bigg)\otimes(\mathbf{V}\times)\Bigg)\mathrm{d}L'
\end{aligned} \tag{19}$$

and $\mathbf{s}^{\mathrm{T}}(\mathbf{x}, t)$ is its transpose. Here, R is the magnitude of $\mathbf{R}$, which is the vector connecting the source point to the observer point, namely, $\mathbf{R} = \mathbf{x} - \mathbf{x}'$.

4.3. Consistency

Different spatial and temporal integration strategies lead to different formulas of the elastodynamics solution (see Equations (16) and (19)). The case of an infinitely long straight dislocation line described in Figure 1a–c schematically shows the difference of the integration strategies. Figure 1b needs to perform temporal integration over each point at different times, while Figure 1c needs to perform spatial integration over the retarded dislocation lines. For 3D dislocation, carrying out the space integration along retarded dislocation is capable of completing calculation of the 3D elastodynamics fields. For 2D dislocation, it is assumed to be along x_3 all the time; the intersection point of the dislocation line and plane Ox_1x_2 can well record the position of dislocation. Performing the straight line integration along the straight dislocation is specific. Thereby, performing the temporal integration can calculate the 2D elastodynamics fields after space integration. It is not apparent to see their physical connections from these figures.

To simplify the discussion and clarify their consistency, the spacial and temporal integration of a basic term is derived as follows, using the integration strategies described in Sections 4.1 and 4.2. If the spatial integration is firstly done,

$$\int_{t_0}^{t}\int_{-\infty}^{\infty} f(\mathbf{x},t')\delta\Big(t-t'-\frac{x}{c}\Big)dx_3dt' = \int_{t_0}^{t}\frac{2xf(\mathbf{x},t')H(t^2-l^2/c^2)}{\sqrt{(t-t')^2-l^2/c^2}}|_{x=c(t-t')}dt' \tag{20}$$

where $x_3\,\epsilon\,[-\sqrt{c^2(t-t_0)^2-l^2}, \sqrt{c^2(t-t_0)^2-l^2}]$, $l^2=(x_1-x_1')^2+(x_2-x_2')^2$.

If the temporal integration is firstly done,

$$\int_{-\infty}^{\infty}\int_{t_0}^{t} f(\mathbf{x},t')\delta\Big(t-t'-\frac{x}{c}\Big)dt'dx_3 = \int_{-\infty}^{\infty} f(\mathbf{x},t')_{t'=t-\frac{x}{c}}dx_3 \tag{21}$$

where $x\,\epsilon\,[0,\ c(t-t_0)]$, therefore $t'=t-\frac{x}{c}\,\epsilon\,[t,t_0]$, mathematically.

Furthermore, $dt'=d(t-\frac{x}{c})=-\frac{dx}{cdx_3}dx_3=-\frac{x_3}{cx}dx_3$. Consequently, Equation (21) becomes

$$\int_{-\infty}^{\infty}\int_{t_0}^{t} f(\mathbf{x},t')\delta\Big(t-t'-\frac{x}{c}\Big)dt'dx_3 = \int_{t_0}^{t}\frac{2xf(\mathbf{x},t')H(t^2-x^2/c^2)}{\sqrt{(t-t')^2-l^2/c^2}}|_{x=c(t-t'))}dt' \tag{22}$$

Equation (22), which firstly calculates the temporal integration, is exactly the same as Equation (20), which firstly carries out the spatial integration. Therefore, for more complex formulas associated with elastodynamics solutions, they are exactly the same.

5. Conclusions

The significant effects of elastodynamics on a dislocation stress field have been recognized for more than 70 years. However, the marked difference in elastodynamics stress expression for 3D and 2D dislocation is seldomly directly discussed. In the current work, the physical origin of their difference and connections is clearly discussed from the perspective of different spatial and temporal decoupling strategies.

For the 2D case, the dislocation configuration keeps straight along a specific direction, which makes it suitable to firstly carry out the spatial integration along its line direction. For the 3D case, the evolution of the dislocation configuration is very complicated, one cannot obtain generalized results if the spatial integration is firstly carried out. Therefore, the temporal integration is firstly performed. The consistency between these two cases is clearly demonstrated through the 2D and 3D elastodynamics Green tensor and a simple generalized formula. This work helps to understand the difference and connections between 2D and 3D dislocation elastodynamics, which leads to an enlightening opportunity for establishing general high-speed dislocation theory, developing a numerical calculation method based on dislocation elastodynamics, and understanding the collective behavior of high-speed dislocations under complicated shock-loading conditions.

Author Contributions: S.L.: Formal analysis, Verification, Writing—review and editing. Y.C.: Conceptualization, Supervision, Formal analysis, Writing—original draft, review, and editing. All authors have read and agreed to the published version of the manuscript.

Funding: This research was supported by the National Natural Science Foundation of China under Grant No. 11972208, 11921002, National Key Laboratory of Shock Wave and Detonation Physics under Grant No. JCKYS2021212004 and Tsinghua University Initiative Scientific Research Program.

Data Availability Statement: Not applicable.

Acknowledgments: We greatly thank M. Lazar, Nasr Ghoniem, and Giacomo Po for the insightful discussions.

Conflicts of Interest: The authors declare no conflict of interest.

Appendix A

Calculating the space integral over 3D Green function in the x_3 direction and 2D elastodynamicss field, we used the following auxiliary formula, where $x = \sqrt{x_1^2 + x_2^2 + x_3^2}$, $l = \sqrt{x_1^2 + x_2^2}$, $x_i (i = 1, 2, 3)$, and $x_\alpha (\alpha = 1, 2)$ are the Cartesian coordinate components, and c_T and c_L are shear and longitudinal wave velocities of the material.

$$\begin{aligned}
&\int_{-\infty}^{\infty} \frac{\delta\left(t - \frac{x}{c}\right)}{x} dx_3 = \frac{1}{x\frac{1}{c}\frac{dx}{dx_3}}\Big|_{x=ct} = \frac{2}{x\frac{1}{c}\frac{x_3}{x}}\Big|_{x=ct} = \frac{2}{\sqrt{t^2 - l^2/c^2}} \\
&\int_{-\infty}^{\infty} \frac{\delta\left(t - \frac{x}{c}\right)}{x^3} dx_3 = \frac{2}{c^2 t^2 \sqrt{t^2 - l^2/c^2}} \\
&\int_{-\infty}^{\infty} \frac{x_\alpha x_3 \delta\left(t - \frac{x}{c}\right)}{x^3} dx_3 = \frac{2x_\alpha}{ct^2} \\
&\int_{-\infty}^{\infty} \frac{x_3^2 \delta\left(t - \frac{x}{c}\right)}{x^3} dx_3 = \frac{2\sqrt{t^2 - l^2/c^2}}{t^2} \\
&\int_{-\infty}^{\infty} \frac{x_3^2 \delta\left(t - \frac{x}{c}\right)}{x^5} dx_3 = \frac{2\sqrt{t^2 - l^2/c^2}}{c^2 t^4} \\
&\int_{-\infty}^{\infty} \frac{x_3^3 \delta\left(t - \frac{x}{c}\right)}{x^5} dx_3 = \frac{2(t^2 - l^2/c^2)}{ct^4} \\
&\int_{-\infty}^{\infty} \frac{x_3 \delta\left(t - \frac{x}{c}\right)}{x^2} dx_3 = \frac{2}{t}
\end{aligned} \tag{A1}$$

$$\begin{aligned}
&\int_{-\infty}^{\infty} \frac{1}{x^3} \int_{x/c_L}^{x/c_T} \tau \delta(t - \tau) d\tau dx_3 = \frac{1}{x} \int_{1/c_L}^{1/c_T} \int_{-\infty}^{\infty} \kappa \delta(t - x\kappa) dx_3 d\kappa \\
&= -\frac{2}{l^2}\sqrt{t^2 - l^2/c_T^2} + \frac{2}{l^2}\sqrt{t^2 - l^2/c_L^2} \\
&\int_{-\infty}^{\infty} \frac{1}{x^5} \int_{x/c_L}^{x/c_T} \tau \delta(t - \tau) d\tau dx_3 = -\frac{4}{3l^4 t^2}\left(t^2 - \frac{l^2}{c_T^2}\right)^{3/2} + \frac{4}{3l^4 t^2}\left(t^2 - \frac{l^2}{c_L^2}\right)^{3/2} \\
&- \frac{2}{l^2 c_T^2 t^2}\sqrt{t^2 - \frac{l^2}{c_T^2}} + \frac{2}{l^2 c_L^2 t^2}\sqrt{t^2 - \frac{l^2}{c_L^2}} \\
&\int_{-\infty}^{\infty} \frac{1}{x^7} \int_{x/c_L}^{x/c_T} \tau \delta(t - \tau) d\tau dx_3 = -\frac{2\sqrt{t^2 - l^2/c_T^2}}{15l^4}\left(8 + \frac{4l^2}{c_T^2 t^2} + \frac{3l^4}{c_T^4 t^4}\right) \\
&+ \frac{2\sqrt{t^2 - l^2/c_L^2}}{15l^4}\left(8 + \frac{4l^2}{c_L^2 t^2} + \frac{3l^4}{c_L^4 t^4}\right)
\end{aligned} \tag{A2}$$

$$
\begin{aligned}
&\int_{-\infty}^{\infty} \frac{x_\alpha x_3}{x^5} \int_{x/c_L}^{x/c_T} \tau\delta(t-\tau)d\tau dx_3 = \frac{2x_\alpha}{3t^2}\left(\frac{1}{c_T^3}-\frac{1}{c_L^3}\right)\\
&\int_{-\infty}^{\infty} \frac{x_3^2}{x^5} \int_{x/c_L}^{x/c_T} \tau\delta(t-\tau)d\tau dx_3 = -\frac{2}{3l^2t^2}\sqrt{(t^2-l^2/c_T^2)^3}+\frac{2}{3l^2t^2}\sqrt{(t^2-l^2/c_L^2)^3}\\
&\int_{-\infty}^{\infty} \frac{x_3^2}{x^7} \int_{x/c_L}^{x/c_T} \tau\delta(t-\tau)d\tau dx_3 = -\frac{2}{5}\left(\frac{1}{l^2c_T^2t^4}+\frac{2}{3l^4t^2}\right)\left(t^2-\frac{l^2}{c_T^2}\right)^{3/2}\\
&+\frac{2}{5}\left(\frac{1}{l^2c_L^2t^4}+\frac{2}{3l^4t^2}\right)\left(t^2-\frac{l^2}{c_L^2}\right)^{3/2}\\
&\int_{-\infty}^{\infty} \frac{x_3^3}{x^7} \int_{x/c_L}^{x/c_T} \tau\delta(t-\tau)d\tau dx_3 = -\frac{\sqrt{t^2-l^2/c_T^2}}{15}\left(\frac{2}{l^4}+\frac{1}{c_T^2l^2t^2}-\frac{3}{c_T^4t^4}\right)\\
&+\frac{\sqrt{c_L^2t^2-l^2}}{15c_L^5l^4t^4}\left(2c_L^4t^4+c_L^2l^2t^2-3l^4\right)
\end{aligned}
\tag{A3}
$$

$$
\begin{aligned}
&\left(\int_{-\infty}^{\infty} \frac{\delta\left(t-\frac{x}{c}\right)}{x^2}dx_3\right)_{,t} = \frac{-4c^2t+2l^2}{t^2\sqrt{(c^2t^2-l^2)^3}}\\
&\left(\int_{-\infty}^{\infty} \frac{\delta\left(t-\frac{x}{c}\right)}{x^4}dx_3\right)_{,t} = \frac{-8c^2t^2+6l^2}{c^2t^4\sqrt{(c^2t^2-l^2)^3}}\\
&\left(\int_{-\infty}^{\infty} \frac{1}{x^3} \int_{x/c_L}^{x/c_T} \tau\delta(t-\tau)d\tau dx_3\right)_{,t} = -\frac{2t}{l^2\sqrt{t^2-l^2/c_T^2}}+\frac{2t}{l^2\sqrt{t^2-l^2/c_L^2}}\\
&\left(\int_{-\infty}^{\infty} \frac{x_3^2\delta\left(t-\frac{x}{c}\right)}{x^4}dx_3\right)_{,t} = \left(\frac{2\sqrt{t^2-l^2/c^2}}{ct^3}\right)_{,t} = \frac{2}{ct^2\sqrt{t^2-l^2/c^2}}-\frac{6\sqrt{t^2-l^2/c^2}}{ct^4}\\
&\left(\int_{-\infty}^{\infty} \frac{x_3^2}{x^5} \int_{x/c_L}^{x/c_T} \tau\delta(t-\tau)d\tau dx_3\right)_{,t} = \frac{4}{3l^2t^3}\sqrt{(t^2-l^2/c_T^2)^3}-\frac{2}{l^2t}\sqrt{t^2-l^2/c_T^2}\\
&-\frac{4}{3l^2t^3}\sqrt{(t^2-l^2/c_L^2)^3}+\frac{2}{l^2t}\sqrt{t^2-l^2/c_L^2}
\end{aligned}
\tag{A4}
$$

References

1. Gray, G.T., III. High-strain-rate deformation: Mechanical behavior and deformation substructures induced. *Annu. Rev. Mater. Res.* **2012**, *42*, 285–303. [CrossRef]
2. Yaghoobi, M.; Voyiadjis, G.Z.; Sundararaghavan, V. Crystal Plasticity Simulation of Magnesium and Its Alloys: A Review of Recent Advances. *Crystals* **2021**, *11*, 435. [CrossRef]
3. Ma, M.; Ding, H.; Huang, Y.; Tian, C.W.; Langdon, T.G. Microstructural and Hardness Evolution in a Duplex Stainless Steel Processed by High-Pressure Torsion. *Crystals* **2020**, *10*, 1138. [CrossRef]
4. Javanbakht, M. High pressure phase evolution under hydrostatic pressure in a single imperfect crystal due to nanovoids. *Materialia* **2021**, *20*, 101199. [CrossRef]
5. Roy, A.M. Barrierless melt nucleation at solid-solid interface in energetic nitramine octahydro-1, 3, 5, 7-tetranitro-1, 3, 5, 7-tetrazocine. *Materialia* **2021**, *15*, 101000. [CrossRef]
6. Meyers, M.A. *Dynamic Behavior of Materials*; John Wiley & Sons: Hoboken, NJ, USA, 1994.
7. Bisht, A.; Neogi, A.; Mitra, N.; Jagadeesh, G.; Suwas, S. Investigation of the elastically shock-compressed region and elastic–plastic shock transition in single-crystalline copper to understand the dislocation nucleation mechanism under shock compression. *Shock Waves* **2019**, *29*, 913–927. [CrossRef]
8. Sichani, M.M.; Spearot, D.E. A molecular dynamics study of dislocation density generation and plastic relaxation during shock of single crystal Cu. *J. Appl. Phys.* **2016**, *120*, 045902. [CrossRef]
9. Tanguy, D.; Mareschal, M.; Lomdahl, P.S.; Germann, T.C.; Holian, B.L.; Ravelo, R. Dislocation nucleation induced by a shock wave in a perfect crystal: Molecular dynamics simulations and elastic calculations. *Phys. Rev. B* **2003**, *68*, 165–168. [CrossRef]
10. Zepeda-Ruiz, L.A.; Stukowski, A.; Oppelstrup, T.; Bulatov, V.V. Probing the limits of metal plasticity with molecular dynamics simulations. *Nature* **2017**, *550*, 492–495. [CrossRef] [PubMed]

11. Eshelby, J. Uniformly Moving Dislocations. *Proc. Phys. Soc.* **1949**, *62*, 307. [CrossRef]
12. Frank, F.C. On the Equations of Motion of Crystal Dislocations. *Proc. Phys. Soc. Sect. A* **1949**, *62*, 131–134. [CrossRef]
13. Markenscoff, X.; Clifton, R. The nonuniformly moving edge dislocation. *J. Mech. Phys. Solids* **1981**, *29*, 253–262. [CrossRef]
14. Nosenko, V.; Zhdanov, S.; Morfill, G. Supersonic dislocations observed in a plasma crystal. *Phys. Rev. Lett.* **2007**, *99*, 25002. [CrossRef]
15. Cui, Y.; Po, G.; Pellegrini, Y.P.; Lazar, M.; Ghoniem, N. Computational 3-dimensional dislocation elastodynamics. *J. Mech. Phys. Solids* **2019**, *126*, 20–51. [CrossRef]
16. Gurrutxaga-Lerma, B.; Balint, D.S.; Dini, D.; Eakins, D.E.; Sutton, A.P. A dynamic discrete dislocation plasticity method for the simulation of plastic relaxation under shock loading. *R. Soc. Math. Phys. Eng. Sci.* **2013** , *469*, 20130141. [CrossRef]
17. Gurrutxaga-Lerma, B.; Balint, D.S.; Dini, D.; Sutton, A.P. Elastodynamic image forces on dislocations. *R. Soc. Math. Phys. Eng. Sci.* **2015** , *471*, 20150433. [CrossRef] [PubMed]
18. Blaschke, D.N. A general solution for accelerating screw dislocations in arbitrary slip systems with reflection symmetry. *J. Mech. Phys. Solids* **2021**, *152*, 104448. [CrossRef]
19. Cui, Y.; Wang, T.; Luo, S.; Li, Z.; Li, Z. A discrete–continuous model of three-dimensional dislocation elastodynamics. *Int. J. Plast.* **2022**, *152*, 103221. [CrossRef]
20. Pellegrini, Y.P.; Lazar, M. On the gradient of the Green tensor in two-dimensional elastodynamic problems, and related integrals: Distributional approach and regularization, with application to nonuniformly moving sources. *Wave Motion* **2015**, *57*, 44–63. [CrossRef]
21. Bringa, E.M.; Rosolankova, K.; Rudd, R.E.; Remington, B.A.; Wark, J.S.; Duchaineau, M.; Kalantar, D.H.; Hawreliak, J.; Belak, J. Shock deformation of face-centred-cubic metals on subnanosecond timescales. *Nat. Mater.* **2006**, *5*, 805–809. [CrossRef]
22. Chu, H.J.; Wang, J.; Beyerlein, I.J. Anomalous reactions of a supersonic coplanar dislocation dipole: Bypass or twinning? *Scr. Mater.* **2012**, *67*, 69–72. [CrossRef]
23. Gumbsch, P.; Gao, H. Dislocations faster than the speed of sound. *Science* **1999**, *283*, 965–968. [CrossRef] [PubMed]
24. Li, Q.J.; Li, J.; Shan, Z.W.; Ma, E. Strongly correlated breeding of high-speed dislocations. *Acta Mater.* **2016**, *119*, 229–241. [CrossRef]
25. Kim, S.; Kim, H.; Kang, K.; Kim, S.Y. Relativistic effect inducing drag on fast-moving dislocation in discrete system. *Int. J. Plast.* **2019**, *126*, 102629. [CrossRef]
26. Cottrell, A.H. Theory of dislocations. *Prog. Met. Phys.* **1968**, *1*, 77–96. [CrossRef]
27. Jin, Z.; Gao, H.; Gumbsch, P. Energy radiation and limiting speeds of fast moving edge dislocations in tungsten. *Phys. Rev. B* **2008**, *77*, 094303. [CrossRef]
28. Tsuzuki, H.; Branicio, P.S.; Rino, J.P. Molecular dynamics simulation of fast dislocations in copper. *Acta Mater.* **2009**, *57*, 1843–1855. [CrossRef]
29. Zhang, X.; Acharya, A.; Walkington, N.J.; Bielak, J. A single theory for some quasi-static, supersonic, atomic, and tectonic scale applications of dislocations. *J. Mech. Phys. Solids* **2015**, *84*, 145–195. [CrossRef]
30. Lazar, M. The gauge theory of dislocations: A uniformly moving screw dislocation. *R. Soc. Lond. A Math. Phys. Eng. Sci.* **2009**, *465*, 2505–2520 [CrossRef]
31. Lazar, M.; Pellegrini, Y.P. Distributional and regularized radiation fields of non-uniformly moving straight dislocations, and elastodynamic Tamm problem. *J. Mech. Phys. Solids* **2016**, *96*, 632–659. [CrossRef]
32. Chen, H.; Levitas, V.I.; Xiong, L.; Zhang, X. Stationary Dislocation Motion at Stresses Significantly below the Peierls Stress: Example of Shuffle Screw and 60 Dislocations in Silicon. *Acta Mater.* **2021**, *206*, 116623. [CrossRef]
33. Li, Q.J.; Li, J.; Shan, Z.W.; Ma, E. Surface Rebound of Relativistic Dislocations Directly and Efficiently Initiates Deformation Twinning. *Phys. Rev. Lett.* **2018**, *117*, 165501. [CrossRef]
34. Markenscoff, X. Evolution equation of moving defects: Dislocations and inclusions. *Int. J. Fract.* **2010**, *166*, 35–40. [CrossRef]
35. Lazar, M. The fundamentals of non-singular dislocations in the theory of gradient elasticity: Dislocation loops and straight dislocations. *Int. J. Solids Struct.* **2013**, *50*, 352–362. [CrossRef]
36. Lazar, M.; Kirchner, H.O.K. Generalised plane strain embedded in three-dimensional anisotropic elasticity. *Philos. Mag.* **2021**, *101*, 2584–2598. [CrossRef]
37. Mura, T. Continuous distribution of moving dislocations. *Philos. Mag.* **1963**, *8*, 843–857. [CrossRef]
38. Callias, C.; Markenscoff, X.; Ni, L.Q. A singular asymptotic expansion for the field near a moving dislocation loop. *Q. Appl. Math.* **1990**, *48*, 113–132. [CrossRef]
39. Lazar, M. On the non-uniform motion of dislocations: The retarded elastic fields, the retarded dislocation tensor potentials and the Liénard—Wiechert tensor potentials. *Philos. Mag.* **2013**, *93*, 749–776. [CrossRef]
40. Eringen, A.C.; Suhubi, E.S.; Bland, D.R. Elastodynamics, vols. 1 and 2. *Phys. Today* **1977**, *30*, 65. [CrossRef]
41. Achenbach, J.D. *Reciprocity in Elastodynamics*; Cambridge University Press: Cambridge, MA, USA, 2003.
42. Jackson, J.D. *Classical Electrodynamics*; John Wiley & Sons: Hoboken, NJ, USA, 2012.